THE JOURNAL OF PHYSICAL CHEMISTRY Letters

pubs.acs.org/JPCL

Letter

Room Temperature Zero Thermal Expansion in a Cubic Cobaltite

Zhijian Tan, Ping Miao,* Masato Hagihala, Sanghyun Lee, Yoshihisa Ishikawa, Shuki Torii, Masao Yonemura, Takashi Saito, Sihao Deng, Jie Chen, Lunhua He, Rong Du, Junrong Zhang, Haisheng Li, Junliang Sun, Yingxia Wang, Xiaohuan Lin, Kuo Li, and Takashi Kamiyama*

HPSTAR 1014-2020

Cite This: *J. Phys. Chem. Lett.* 2020, 11, 6785−6790

Read Online

ACCESS | Metrics & More | Article Recommendations | Supporting Information

ABSTRACT: Zero thermal expansion (ZTE) materials are highly desired in modern industries where high-precision processing is necessary. However, ZTE materials in pure form are extremely rare. The most widely used are Invar alloys, where the ZTE is intimately associated with spontaneous magnetic ordering, known as the magneto-volume effect (MVE). Despite tremendous studies, there is still no consensus on the microscopic origin of MVE in Invar alloys. Here, we report the discovery of room-temperature isotropic ZTE in a pure-form cobaltite perovskite, A-site disordered $La_{0.5}Ba_{0.5}CoO_{3-x}$. The temperature window of the anomalous thermal expansion shows large tunability by simply altering the oxygen content, making this material a promising candidate for practical applications. Furthermore, we unveil with compelling experimental evidence that the ZTE originates from an isostructural transition between antiferromagnetic large-volume phase and ferromagnetic small-volume phase, which might shed light on the MVE in Invar alloys.

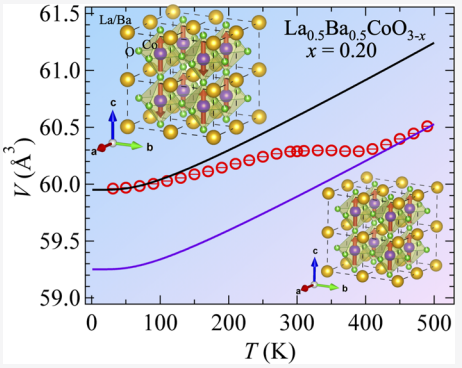

Most materials show positive thermal expansion (PTE) due to anharmonic vibrations of atoms,[1−3] which can be described by the Debye−Grüneisen model.[4] However, some materials deviate from the model and exhibit anomalous thermal expansion (ATE), such as negative thermal expansion (NTE) and zero thermal expansion (ZTE). ZTE materials which are invariable in volume over a certain temperature range are attracting considerable interest because of their potential applications in precision devices, optics, and electronics, where dimensional instability induced by thermal fluctuation should be avoided.[3,5,6]

Most ZTE materials are fabricated by combining normal PTE compounds with NTE compounds. However, in such ZTE composites, severe microcracks are often induced by stress occurring at interfaces or grain boundaries, which significantly diminish their mechanical performance and lifetime. The problem can be overcome if ZTE is realized in a pure-form compound. Only a small number of such compounds has been discovered so far, such as Invar alloys,[7,8] $Fe[Co(CN)_6]$,[9] antiperovskite manganese nitride,[10] $(Zr,Nb)Fe_2$,[11] $PbTiO_3$-based perovskites,[12,13] and $Zr_{0.6}Sn_{0.4}Mo_2O_8$.[14] Furthermore, to meet the requirement for practical applications, it is crucial that the ZTE occurs in an isotropic manner and within a temperature window spanning room temperature.

To date, the only pure-form ZTE materials that find wide applications are Invar alloys. The ZTE in Invar alloys is known as the Invar effect, first discovered by Guillaume in $Fe_{0.65}Ni_{0.35}$ alloy that bears an extremely low linear coefficient of thermal expansion, $\alpha = 1.2 \times 10^{-6}$ K^{-1}, at room temperature.[7] The Invar alloys have attracted much attention not only because of their broad applications but also due to the mysterious underlying mechanism. Although it has long been known that the Invar effect is intimately connected with spontaneous magnetic ordering, called the magnetovolume effect (MVE),[15] the microscopic origin of the MVE is still under debate.[15−18] Since the discovery of MVE in $Fe_{0.65}Ni_{0.35}$ alloy, MVE has been found in various materials that show ATE, such as Mn_3AN(A = Zn,Ga, etc.),[19−21] $Ho_2Fe_{16}Cr$,[22] La(Fe,Si,Co),[23] Mn_3Ge,[24] MnCoGe,[25,26] R_2Fe_{17} (R = rare earth elements),[27] Tb-$(Co,Fe)_2$,[28] and TFe_2 (T = transition metal elements).[11,29,30] The mechanism of MVE varies in different compounds, leading to new and emergent physics.

In the present work, we report a new class of pure-form ZTE material, A-site disordered perovskite $La_{0.5}Ba_{0.5}CoO_{3-x}$, in which an ultralow α of -1.32×10^{-7} K^{-1} around room temperature (290−410 K) is observed at $x = 0.20$, as shown in Figure 1(a). Also, the thermal expansion property demonstrates wide and easy tunability. By simply altering the oxygen deficiency x, the α value changes significantly, and the temperature window of ATE shifts as well [Figure 1(a) and (b)], so that the ATE spans a large region of $T-x$ phase diagram [Figure 1(c)]. It is worth noting that, as illustrated in

Received: June 20, 2020
Accepted: July 23, 2020
Published: July 23, 2020

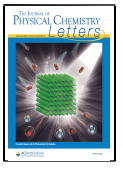

https://dx.doi.org/10.1021/acs.jpclett.0c01919
J. Phys. Chem. Lett. 2020, 11, 6785−6790

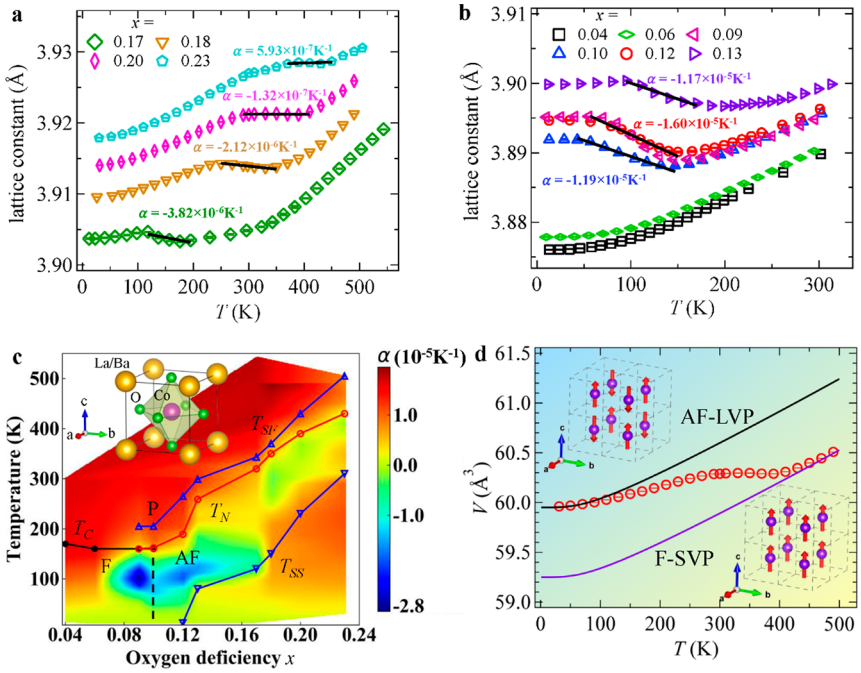

Figure 1. Lattice constant (a, b), phase diagram (c), and phase transition model (d) of $La_{0.5}Ba_{0.5}CoO_{3-x}$. (a and b) Lattice constant as a function of temperature for various oxygen deficiency x measured by neutron powder diffraction. The neutron results are in good agreement with the macroscopic dilatometry measurement as shown in Figure S10. α denotes the linear coefficient of thermal expansion, showing ATE of different magnitudes and at different temperature windows depending on the x. The neutron (c) $T-x$ phase diagram for $La_{0.5}Ba_{0.5}CoO_{3-x}$. The results are summarized from the neutron powder diffraction study. P, AF, and F denote the paramagnetic state, antiferromagnetic state, and ferromagnetic state, respectively. T_C and T_N are determined by the appearance of long-range ordered magnetic peaks. T_{SS} and T_{SF} represent the starting and ending temperature of the phase transition, respectively, derived from the analysis of relative Bragg peak breadth fwhm/d. A contour colored plot describes the α values at different T and x. The inset illustrates the cubic perovskite structure, which is retained throughout the $T-x$ phase diagram. (d) The phase transition model for the ATE. The LVP is characterized by the AF (G-type) structure of Co spins (the upper-left inset) at ground state, while the SVP has the F structure (the lower-right inset). Both phases follow the Debye–Grüneisen model, showing PTE, and the ATE comes from the transition from AF-LVP to F-SVP upon heating.

the inset of Figure 1(c), the crystal structure of $La_{0.5}Ba_{0.5}CoO_{3-x}$ remains cubic perovskite with the space group $Pm\bar{3}m$ throughout $T-x$ phase diagram, i.e., the ATE occurs isotropically, which constitutes another benefit for practical applications. Furthermore, our experimental evidence in this research reveals that analogous to the Invar alloys, the ATE in the $La_{0.5}Ba_{0.5}CoO_{3-x}$ also arise from the MVE. By carefully studying the crystal and magnetic structures, we found the MVE is closely related to the competition between ferromagnetic small-volume phase (F-SVP) and antiferromagnetic large-volume phase (AF-LVP). Both phases follow the Debye–Grüneisen model,[4] exhibiting normal positive thermal expansion, and the ATE originates from the transition between AF-LVP to F-SVP, as depicted in Figure 1(d). Especially, when the reduction in volume from AF-LVP–F-SVP transition compensates the volume expansion from anharmonic vibrations of atoms, the ZTE is therefore realized.

Utilizing the high-resolution neutron powder diffractometer, SuperHRPD, we obtained evidence for phase conversion between AF-LVP and F-SVP. As shown in Figure 2(a), nuclear reflection (111) of the x = 0.10 sample manifests itself as a single peak at high temperatures, but a new peak with larger d-spacing starts to appear at about 162 K upon cooling, whose intensity grows at the expense of the original peak until base temperature. This peak splitting occurs in all Bragg peaks, as shown in Figure S3, which rules out the possibility of symmetry breaking of the crystal structure and instead indicates a transition from a high-temperature small-volume phase to a low-temperature large-volume phase. The phase transition does not finish down to the base temperature because a small portion of small-volume phase still survives, so that we cannot define the starting temperature T_{SS} of phase transition. From the temperature dependence of relative full width at half-maximum (fwhm/d) of reflection (111), as shown in Figure 2(d), we found peak broadening caused by the large-volume phase when its portion is small. The peak broadening survives until about 210 K upon heating, defining the ending temperature of phase transition T_{SF}. The phase coexistence during the transition in terms of peak splitting was also observed in samples of different oxygen content (x = 0.09, 0.12, 0.13, and 0.17), as shown in Figures S2 and S3.

On the other hand, we found that the small-volume phase and the large-volume phase are coupled with ferromagnetic (F) and antiferromagnetic (AF) ordering, respectively. As shown in Figure 2(b), the increase in intensity of the reflection (100) initiating from 160 K upon cooling indicates the ferromagnetic ordering with propagation vector k_F = (0, 0, 0), while the superlattice reflections $\left(\frac{1}{2}\frac{1}{2}\frac{1}{2}\right)$ initiating at similar temperatures signify the AF ordering with propagation vector k_{AF} = $\left(\frac{1}{2}, \frac{1}{2}, \frac{1}{2}\right)$. The magnetization properties also suggest the coexistence of F and AF ordering at low temperatures. As shown in Figure S5(b), below 130 K, the decrease of magnetization under the field cooling (FC) process upon cooling suggests the AF correlation, while the difference between the magnetization of zero-field cooling (ZFC) and FC

https://dx.doi.org/10.1021/acs.jpclett.0c01919
J. Phys. Chem. Lett. 2020, 11, 6785–6790

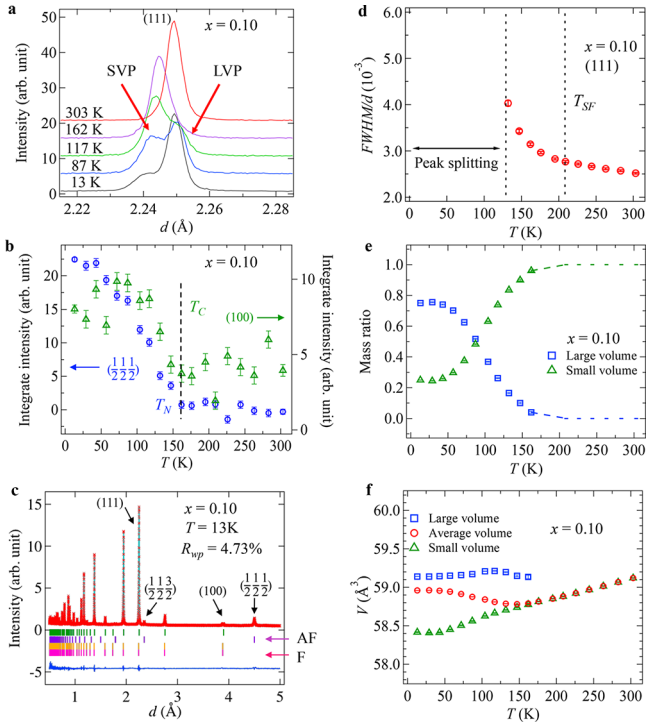

Figure 2. High-resolution neutron powder diffraction on $La_{0.5}Ba_{0.5}CoO_{3-x}$ (x = 0.10). (a) Diffraction patterns of the reflection (111) at different temperatures. Peak splitting occurs in reflection (111) at low temperatures, indicating coexistence of LVP and SVP. (b) Temperature dependences of integrated intensities of the AF reflection $\left(\frac{1}{2}\frac{1}{2}\frac{1}{2}\right)$ and F reflection (100). (c) Rietveld refinement on the pattern at 13 K by using the model of double phases, i.e., AF-LVP and F-SVP. The observed and calculated patterns are shown at the top with the red markers and the solid line, respectively. The green (purple) bars in the middle denote the indices from nuclear (magnetic) structures of AF-LVP, while the orange (magenta) bars represent the indices from nuclear (magnetic) structures of F-SVP. The bottom blue line represents the difference between observed and calculated intensities. The residual values R_{wp} is 4.73% and R_M is 9.8 and 31.2% for AF and F, respectively. (d) Relative peak breadth fwhm/d of nuclear reflection (111) at high temperatures before splitting into two upon cooling. The decrease in fwhm/d as the temperature increases is associate with the final stage of the conversion from LVP to SVP, where LVP exists in a short-range scale. Therefore, the temperature where fwhm/d drops to a nearly flat level is defined as the final transition temperature T_{SF}. (e) Mass ratios as a function of temperature were obtained from Rietveld refinement. (f) Unit cell volumes as a function of temperature were obtained from Rietveld refinement. The average unit cell volume is calculated by $V_{average} = V_{LVP}V_{LVP} + V_{SVP}V_{SVP}$, where R is the mass ratio.

process and the hysteresis loop in the magnetization as a function of magnetic field (M/H curve) (see in the inset of Figure S5(b)) at 10 K are indicative of the F correlation. With the $Pm\bar{3}m$ cubic crystal structure and magnetic propagation vector of the two phases, we performed the symmetry analysis based on the representation theory and obtained the symmetry-allowed magnetic structures, as shown in Tables S1 and S2. Through Rietveld refinement, we finally determined that the two-phase model of AF-LVP and F-SVP, where the G-type AF structure and F structure are depicted in the inset of Figure 1(d), can best describe the pattern of x = 0.10 at 13 K, as shown in Figure 2(c). Based on the resultant mass ratio and unit cell volume for each phase, we derived the average volume as a function of temperature, which exhibits NTE from around 50 to 140 K, as shown in Figure 2(e) and Figure 2(f).

More evidence for the magnetoelastic coupling of AF-LVP and F-SVP comes from the magnetic-field neutron powder diffraction. Figure 3 shows the result of the magnetic-field

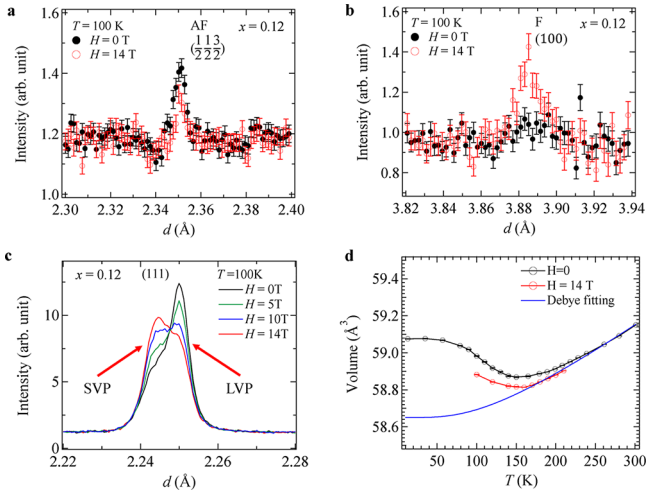

Figure 3. Neutron powder diffraction under magnetic field on $La_{0.5}Ba_{0.5}CoO_{3-x}$ (x = 0.12). (a, b) The diffraction patterns of $La_{0.5}Ba_{0.5}CoO_{3-x}$ (x = 0.12) around AF reflections (a) and F reflections (b) under 0 and 14 T at 100 K. Upon applying 14 T magnetic field at T = 100 K, the AF reflection $\left(\frac{1}{2}\frac{1}{2}\frac{3}{2}\right)$ is suppressed, while the intensity of F reflections (100) significantly increases. (c) The diffraction patterns of nuclear reflection (111) under different magnetic fields at 100 K. The intensity of LVP decreases while the intensity of SVP increases upon applying the field. (d) The average unit cell volumes as a function of temperature under 0 and 14 T. The blue solid line is calculated from the Debye−Grüneisen model. The average unit cell volume under 14 T is suppressed and approaches the calculated value.

NPD for x = 0.12. Upon applying 14 T magnetic field at T = 100 K, the intensities of AF reflection $\left(\frac{1}{2}\frac{1}{2}\frac{3}{2}\right)$ and LVP nuclear reflection (111) decrease while the intensities of F reflection (100) and SVP nuclear reflection (111) significantly increase, as shown in Figure 3(a−c). Therefore, the magnetic field induces phase conversion from AF-LVP and F-SVP. Consequently, the average unit cell volume is suppressed, and the overall NTE is weakened under magnetic field [Figure 3(d)].

Though the splitting of Bragg peaks was not observed in samples with x > 0.17, which also display ATE, as shown in Figure 4(a) and Figure S2(h, j), we still can find the evidence of the coexistence of AF-LVP and F-SVP by analyzing the evolution of peak width as a function of temperature. As depicted in Figure 4(b, c), the fwhm/d of reflection (111) of the sample x = 0.20 increases upon heating from T_{SS} = 230 K, reaches maximum at 370 K, and finally reverts to the normal value at T_{SF} = 430 K. The unusual peak broadening is ubiquitous in all Bragg peaks, as depicted in Figure S4(c, d), indicating that it arises from the lattice inhomogeneity induced by the coexistence of LVP and SVP. The coexistence of F and AF ordering was also observed in neutron diffraction and magnetization, as shown in Figure 4(d). Long-range AF ordering is directly identified by the appearance of the magnetic reflection $\left(\frac{1}{2}\frac{1}{2}\frac{1}{2}\right)$ from diffraction. Though magnetic

https://dx.doi.org/10.1021/acs.jpclett.0c01919
J. Phys. Chem. Lett. 2020, 11, 6785−6790

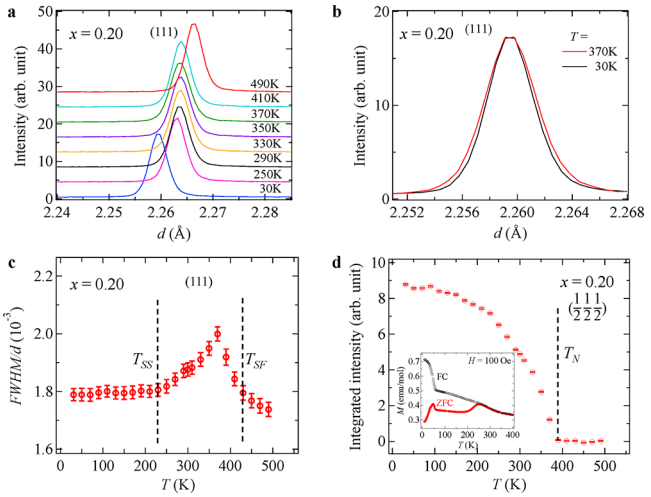

Figure 4. High-resolution neutron powder diffraction on $La_{0.5}Ba_{0.5}CoO_{3-x}$ (x = 0.20). (a) Diffraction patterns of reflection (111) for the samples x = 0.20 at different temperatures. The patterns show single peaks at all the temperature ranges, while they also exhibit nearly no shift of position between 250 to 410 K (ZTE). (b) The comparison of peak width for reflection (111) at 30 and 370 K. For the better comparison, the peaks are shifted to the same position and normalized to the same intensity. It is seen that the peak width at 370 K is broader than that at 30 K, showing that there are more severe lattice inhomogeneities at 370 K. (c) The relative peak breadth fwhm/d of nuclear reflection (111) is a function of temperature. T_{SS} and T_{SF} represent the starting and ending temperature of the phase transition, respectively. The peak broadening which arises from lattice inhomogeneities appears with decreasing temperature, suggesting coexistence of LVP and SVP between 230 and 430 K. The recovery of fwhm/d to normal value indicates the transition between LVP to SVP finishes at temperatures, where a single phase exists. (d) The temperature dependence of integrated intensity of the AF reflection $\left(\frac{1}{2}\frac{1}{2}\frac{1}{2}\right)$. The inset shows the temperature dependence of magnetization under 100 Oe in the ZFC and FC processes, respectively.

peak from long-range F ordering was not observed in diffraction, the difference between the magnetization of ZFC and FC process and the hysteresis loop in the M/H curve at 10 K indicates the F correlation, presumably in short-range order, still exists at low temperatures. Moreover, the temperature window of unusual peak broadening (Figure 4c) coincides with that of ZTE (Figure 1a), reflecting that the ZTE is intimately associated with the conversion between AF-LVP and F-SVP.

In contrast, in the sample x = 0.04, which has single phase and shows normal PTE throughout the measured temperatures, the fwhm/d retains nearly invariant as a function of temperature, as shown in Figure S8(a), further confirming that the unusual peak broadening observed in samples with $x > 0.17$ (Figure S4) is related to the coexistence of AF-LVP and F-SVP.

Up to now, we have demonstrated in the A-site disordered perovskite $La_{0.5}Ba_{0.5}CoO_{3-x}$ the isotropic ATE exists in a large area of the $T-x$ phase diagram, including the ZTE spanning room temperature at x = 0.20. The cobaltite has great advantages for practical use for two reasons: (1) The room-temperature isotropic ZTE in a pure-form compound can be directly applied without suffering microcracks and detriment that often occur during the frequently thermal cycling in the ZTE composite fabricated by combining NTE and PTE materials. In the ZTE composites combining PTE and NTE material, microcracking during repeated thermal cycling may occur due to the stress at the grain boundaries induced by the size mismatch between PTE and NTE grains. However, the pure-form cobaltite perovskite $La_{0.5}Ba_{0.5}CoO_{3-x}$ with isotropic crystal structure is homogeneous in the scale of grain size, so that much less stress exists at the grain boundaries. Inside the grains, stress could be introduced at the boundaries between F-SVP and AF-LVP domains. In comparison with PTE and NTE grains, F-SVP and AF-LVP domains are more closely bonded and in a smaller scale. Therefore, the microcracking problem should be significantly less severe at the boundaries between F-SVP and AF-LVP domains. (2) By tuning the oxygen deficient value x between 0.18 and 0.23, the ZTE can be obtained in a wide temperature window from 250 to 450 K, which could satisfy most industrial demands. $La_{0.5}Ba_{0.5}CoO_{3-x}$ is a rare example of pure-form compound that exhibits isotropic ZTE tunable in a wide temperature window. As far as we know, only a few materials exhibit these properties, such as the Invar alloys,[7,8] the antiperovskite manganese nitride,[10] and (Zr,Nb)-Fe_2.[11]

We have also unveiled with compelling evidence the underlying mechanism of the ATE in $La_{0.5}Ba_{0.5}CoO_{3-x}$ is the phase conversion between AF-LVP and F-SVP. The mechanism is consistent with what we have found in the A-site ordered perovskite with orthorhombic crystal structure, $PrBaCo_2O_{5.5+x}$,[31−33] so that we believe the scenario of AF-LVP−F-SVP transition is ubiquitous in the family of cobaltite perovskite, regardless of A-site ions and its ordering.

$La_{0.5}Ba_{0.5}CoO_{3-x}$ is analogous to the Invar alloys in the following ways: (1) both systems show ATE that is associated with the MVE and (2) both structures are cubic and undergo no change of crystal symmetry throughout the temperature window of ATE. Therefore, our discovery may shed light on the microscopic origin of the Invar effect, which has been under a longstanding debate.[34,35] One of the well-known models is the 2γ-state model,[18] which contains two different magnetic states, the ferromagnetic larger-volume state γ_1 and the antiferromagnetic small-volume state γ_2. However, the existence of the two states has not yet been confirmed experimentally.[15−18] We validate the two-state model in $La_{0.5}Ba_{0.5}CoO_{3-x}$ by directly observing the coexistence of AF-LVP and F-SVP, which was also reported by Troyanchuk.[36]

In summary, we have discovered a new class of pure-form isotropic ATE material in A site-disordered perovskite $La_{0.5}Ba_{0.5}CoO_{3-x}$. The temperature window of ATE is easily tunable by changing the oxygen content and especially the isotropic ZTE for x = 0.20 can be achieved over a broad temperature range (290−410 K), showing high potential for practical applications. We also revealed that the microscopic origin of the ATE lies in the conversion between AF-LVP and F-SVP.

■ ASSOCIATED CONTENT

Supporting Information

The Supporting Information is available free of charge at https://pubs.acs.org/doi/10.1021/acs.jpclett.0c01919.

Methods and neutron powder diffraction and magnetization data for samples with other oxygen contents (PDF)

https://dx.doi.org/10.1021/acs.jpclett.0c01919
J. Phys. Chem. Lett. 2020, 11, 6785−6790

AUTHOR INFORMATION

Corresponding Authors

Ping Miao − *Institute of Materials Structure Science, High Energy Accelerator Research Organization (KEK), Tokai, Ibaraki 319-1106, Japan; Institute of High Energy Physics, Chinese Academy of Sciences, Beijing 100049, China; Spallation Neutron Source Science Center, Dongguan 523803, China;* orcid.org/0000-0003-1937-1736; Email: miaoping@ihep.ac.cn

Takashi Kamiyama − *Institute of Materials Structure Science, High Energy Accelerator Research Organization (KEK), Tokai, Ibaraki 319-1106, Japan; Department of Materials Structure Science, Sokendai (The Graduate University for Advanced Studies), Tokai, Ibaraki 319-1106, Japan;* orcid.org/0000-0002-6359-0445; Email: takashi.kamiyama@kek.jp

Authors

Zhijian Tan − *Institute of Materials Structure Science, High Energy Accelerator Research Organization (KEK), Tokai, Ibaraki 319-1106, Japan; Department of Materials Structure Science, Sokendai (The Graduate University for Advanced Studies), Tokai, Ibaraki 319-1106, Japan; Institute of High Energy Physics, Chinese Academy of Sciences, Beijing 100049, China; Spallation Neutron Source Science Center, Dongguan 523803, China*

Masato Hagihala − *Institute of Materials Structure Science, High Energy Accelerator Research Organization (KEK), Tokai, Ibaraki 319-1106, Japan; Department of Materials Structure Science, Sokendai (The Graduate University for Advanced Studies), Tokai, Ibaraki 319-1106, Japan*

Sanghyun Lee − *Institute of Materials Structure Science, High Energy Accelerator Research Organization (KEK), Tokai, Ibaraki 319-1106, Japan*

Yoshihisa Ishikawa − *Institute of Materials Structure Science, High Energy Accelerator Research Organization (KEK), Tokai, Ibaraki 319-1106, Japan; Neutron Science and Technology Center, CROSS, Tokai, Ibaraki 319-1106, Japan*

Shuki Torii − *Institute of Materials Structure Science, High Energy Accelerator Research Organization (KEK), Tokai, Ibaraki 319-1106, Japan*

Masao Yonemura − *Institute of Materials Structure Science, High Energy Accelerator Research Organization (KEK), Tokai, Ibaraki 319-1106, Japan; Department of Materials Structure Science, Sokendai (The Graduate University for Advanced Studies), Tokai, Ibaraki 319-1106, Japan*

Takashi Saito − *Institute of Materials Structure Science, High Energy Accelerator Research Organization (KEK), Tokai, Ibaraki 319-1106, Japan*

Sihao Deng − *Institute of High Energy Physics, Chinese Academy of Sciences, Beijing 100049, China; Spallation Neutron Source Science Center, Dongguan 523803, China*

Jie Chen − *Institute of High Energy Physics, Chinese Academy of Sciences, Beijing 100049, China; Spallation Neutron Source Science Center, Dongguan 523803, China*

Lunhua He − *Institute of Physics, Chinese Academy of Sciences, Beijing 100190, China; Spallation Neutron Source Science Center, Dongguan 523803, China*

Rong Du − *Institute of High Energy Physics, Chinese Academy of Sciences, Beijing 100049, China; Spallation Neutron Source Science Center, Dongguan 523803, China*

Junrong Zhang − *Institute of High Energy Physics, Chinese Academy of Sciences, Beijing 100049, China; Spallation Neutron Source Science Center, Dongguan 523803, China*

Haisheng Li − *State Key Laboratory for Rare Earth Materials Chemistry and Applications, College of Chemistry and Molecular Engineering, Peking University, Beijing 100871, China*

Junliang Sun − *State Key Laboratory for Rare Earth Materials Chemistry and Applications, College of Chemistry and Molecular Engineering, Peking University, Beijing 100871, China;* orcid.org/0000-0003-4074-0962

Yingxia Wang − *State Key Laboratory for Rare Earth Materials Chemistry and Applications, College of Chemistry and Molecular Engineering, Peking University, Beijing 100871, China;* orcid.org/0000-0002-3324-4832

Xiaohuan Lin − *Center for High Pressure Science and Technology Advanced Research, Beijing 100094, China*

Kuo Li − *Center for High Pressure Science and Technology Advanced Research, Beijing 100094, China;* orcid.org/0000-0002-4859-6099

Complete contact information is available at: https://pubs.acs.org/10.1021/acs.jpclett.0c01919

Notes

The authors declare no competing financial interest.

ACKNOWLEDGMENTS

The neutron diffraction experiments were carried out within S-type research project (2014S05) at Japan Proton Accelerator Research Complex (J-PARC) and under the fast-track proposal of GPPD at the China Spallation Neutron Source (CSNS). The sample synthesis and magnetization measurement were performed at the CROSS user laboratories in Tokai, Japan and Southern University of Science and Technology, China. The dilatometry measurement was carried out at Zhejiang University, China. We would like to thank Kaoru Namba, Masahiro Shioya, Motoyuki Ishikado, Widya Rika Puspita, Nur Ika Puji Ayu, Katsumi Shimizu, Han Ge, Liusuo Wu, Ye Chen, and Huiqiu Yuan for their assistance in experiments.

REFERENCES

(1) Barrera, G. D.; Bruno, J. A. O.; Barron, T. H. K.; Allan, N. L. Negative thermal expansion. *J. Phys.: Condens. Matter* **2005**, *17*, R217−R252.

(2) Kittel, C. *Introduction to Solid State Physics*, 8th ed.; John Wiley & Sons, Inc.: New York, 2004.

(3) Chen, J.; Hu, L.; Deng, J.; Xing, X. Negative thermal expansion in functional materials: controllable thermal expansion by chemical modifications. *Chem. Soc. Rev.* **2015**, *44*, 3522−3567.

(4) Wallace, D. C. *Thermodynamics of Crystals*; Dover Pbulications: New York, 1998.

(5) Evans, J. S. O. Negative thermal expansion materials. *J. Chem. Soc., Dalton Trans.* **1999**, *19*, 3317−3326.

(6) Takenaka, K. Negative thermal expansion materials: technological key for control of thermal expansion. *Sci. Technol. Adv. Mater.* **2012**, *13*, 013001.

(7) Guillaume, C. E. Recherches sur les aciers au nickel. Dilatations aux temperatures elevees; resistance electrique. *C. R. Acad. Sci.* **1897**, *125*, 235.

(8) Mohn, P. A century of zero expansion. *Nature* **1999**, *400*, 18.

(9) Margadonna, S.; Prassides, K.; Fitch, A. N. Zero Thermal expansion in a prussian blue analogue. *J. Am. Chem. Soc.* **2004**, *126*, 15390−15391.

(10) Takenaka, K.; Takagi, H. Zero thermal expansion in a pure-form antiperovskite manganese nitride. *Appl. Phys. Lett.* **2009**, *94*, 131904.

(11) Song, Y.; Sun, Q.; Yokoyama, T.; Zhu, H.; Li, Q.; Huang, R.; Ren, Y.; Huang, Q.; Xing, X.; Chen, J. Transforming thermal

expansion from positive to negative: The case of cubic magnetic compounds of (Zr,Nb)Fe_2. *J. Phys. Chem. Lett.* **2020**, *11*, 1954−1961.
(12) Chen, J.; Xing, X.; Sun, C.; Hu, P.; Yu, R.; Wang, X.; Li, L. Zero thermal expansion in $PbTiO_3$-based perovskites. *J. Am. Chem. Soc.* **2008**, *130*, 1144−1145.
(13) Ren, Z.; Zhao, R.; Chen, X.; Li, M.; Li, X.; Tian, H.; Zhang, Z.; Han, G. Mesopores induced zero thermal expansion in single-crystal ferroelectrics. *Nat. Commun.* **2018**, *9*, 1638.
(14) Tallentire, S. E.; Child, F.; Fall, I.; Vella-Zarb, L.; Evans, I. R.; Tucker, M. G.; Keen, D. A.; Wilson, C.; Evans, J. S. Systematic and controllable negative, zero, and positive thermal expansion in cubic $Zr_{1-x}Sn_xMo_2O_8$. *J. Am. Chem. Soc.* **2013**, *135*, 12849−12856.
(15) Wasserman, E. F. *Ferromagntic Materials, Chapter 3*; Elsevier Science Publisher, B.V., 1990.
(16) Nakamura, Y. The Invar Problem. *IEEE Trans. Magn.* **1976**, *12*, 278.
(17) Weiss, R. J. The Origin of the "Invar" Effect. *Proc. Phys. Soc., London* **1963**, *82*, 281.
(18) Ruban, A. V.; Khmelevskyi, S.; Mohn, P.; Johansson, B. Magnetic state, magnetovolume effects, and atomic order in $Fe_{65}Ni_{35}$ Invar alloy: A first principles study. *Phys. Rev. B: Condens. Matter Mater. Phys.* **2007**, *76*, 014420.
(19) Takenaka, K.; Takagi, H. Giant negative thermal expansion in Ge-doped anti-perovskite manganese nitrides. *Appl. Phys. Lett.* **2005**, *87*, 261902.
(20) Deng, S.; Sun, Y.; Wu, H.; Huang, Q.; Yan, J.; Shi, K.; Malik, M.; Lu, H.; Wang, L.; Huang, R.; Li, L.; Wang, C. Invar-like Behavior of Antiperovskite $Mn_{3+x}Ni_{1-x}N$ Compounds. *Chem. Mater.* **2015**, *27*, 2495−2501.
(21) Guo, X.; Lin, J.; Tong, P.; Wang, M.; Wu, Y.; Yang, C.; Song, B.; Lin, S.; Song, W.; Sun, Y. Magnetically driven negative thermal expansion in antiperovskite $Ga_{1-x}Mn_xN_{0.8}Mn_3$ ($0.1 < x < 0.3$). *Appl. Phys. Lett.* **2015**, *107*, 202406.
(22) Dan, S.; Mukherjee, S.; Mazumdar, C.; Ranganathan, R. Zero thermal expansion with high Curie temperature in $Ho_2Fe_{16}Cr$ alloy. *RSC Adv.* **2016**, *6*, 94809.
(23) Li, S.; Huang, R.; Zhao, Y.; Wang, W.; Han, Y.; Li, L. Zero Thermal Expansion Achieved by an Electrolytic Hydriding Method in La(Fe,Si)$_{13}$ Compounds. *Adv. Funct. Mater.* **2017**, *27*, 1604195.
(24) Song, Y.; Qiao, Y.; Huang, Q.; Wang, C.; Liu, X.; Li, Q.; Chen, J.; Xing, X. Opposite Thermal Expansion in Isostructural Non-collinear Antiferromagnetic Compounds of Mn_3A (A = Ge and Sn). *Chem. Mater.* **2018**, *30*, 6236−6241.
(25) Zhao, Y.; Hu, F.; Bao, L.; Wang, J.; Wu, H.; Huang, Q.; Wu, R.; Liu, Y.; Shen, F.; Kuang, H.; Zhang, M.; Zuo, W.; Zheng, X.; Sun, J.; Shen, B. Giant Negative Thermal Expansion in Bonded MnCoGe-Based Compounds with Ni_2In-Type Hexagonal Structure. *J. Am. Chem. Soc.* **2015**, *137*, 1746−1749.
(26) Ren, Q.; Hutchison, W.; Wang, J.; Studer, A.; Wang, G.; Zhou, H.; Ma, J.; Campbell, S. Negative Thermal Expansion of Ni-Doped MnCoGe at RoomTemperature Magnetic Tuning. *ACS Appl. Mater. Interfaces* **2019**, *11*, 17531−17538.
(27) Álvarez, P.; Gorria, P.; Marcos, J.; Orench, I.; Velamazán, J.; Cuello, G.; Llamazares, J.; Blanco, J. Magnetic structure and magneto-volume anomalies in Er_2Fe_{17} compound. *J. Phys.: Condens. Matter* **2011**, *325*, 012011.
(28) Song, Y.; Chen, J.; Liu, X.; Wang, C.; Zhang, J.; Liu, H.; Zhu, H.; Hu, L.; Lin, K.; Zhang, S.; Xing, X. Zero Thermal Expansion in Magnetic and Metallic Tb(Co,Fe)$_2$ Intermetallic Compounds. *J. Am. Chem. Soc.* **2018**, *140* (2), 602−605.
(29) Song, Y.; Sun, Q.; Xu, M.; Zhang, J.; Hao, Y.; Qiao, Y.; Zhang, S.; Huang, Q.; Xing, X.; Chen, J. Negative thermal expansion in (Sc,Ti)Fe_2 induced by an unconventional magnetovolume effect. *Mater. Horiz.* **2020**, *7*, 275−281.
(30) Song, Y.; Chen, J.; Liu, X.; Wang, C.; Gao, Q.; Li, Q.; Hu, L.; Zhang, J.; Zhang, S.; Xing, X. Structure, Magnetism, and Tunable Negative Thermal Expansion in (Hf, Nb)Fe_2 Alloys. *Chem. Mater.* **2017**, *29*, 7078−7082.
(31) Miao, P.; Tan, Z.; Lee, S.; Ishikawa, Y.; Torii, S.; Yonemura, M.; Koda, A.; Komatsu, K.; Machida, S.; Sano-Furukawa, A.; Hattori, T.; Lin, X.; Li, K.; Mochiku, T.; Kikuchi, R.; Kawashima, C.; Takahashi, H.; Huang, Q.; Itoh, S.; Kadono, R.; Wang, Y.; Pan, F.; Yamauchi, K.; Kamiyama, T. Origin of magnetovolume effect in a cobaltite. *arXiv:* **2020**, *2003*, 07567.
(32) Miao, P.; Lin, X.; Lee, S.; Ishikawa, Y.; Torii, S.; Yonemura, M.; Ueno, T.; Inami, N.; Ono, K.; Wang, Y.; Kamiyama, T. Hole-doping-induced melting of spin-state ordering in $PrBaCo_2O_{5.5+x}$. *Phys. Rev. B: Condens. Matter Mater. Phys.* **2017**, *95*, 125123.
(33) Miao, P.; Lin, X.; Koda, A.; Lee, S.; Ishikawa, Y.; Torii, S.; Yonemura, M.; Mochiku, T.; Sagayama, H.; Itoh, S.; Ikeda, K.; Otomo, T.; Wang, Y.; Kadono, R.; Kamiyama, T. Large magneto-volume effect induced by embedding ferromagnetic clusters into antiferromagnetic matrix of cobaltite perovskite. *Adv. Mater.* **2017**, *29*, 1605991.
(34) Johnson, D. D.; Shelton, W. A. In The Invar effect: A Centennial Symposium. *The Minerals, Metals & Materials Soc.*; Wittenauer, J., Ed.; Warrendale, PA, pp 63−74, 1997.
(35) Van Schilfgaarde, M.; Abrikosov, I. A.; Johansson, B. Origin of the Invar effect in iron-nickel alloys. *Nature* **1999**, *400*, 46−49.
(36) Troyanchuk, I. O.; Karpinsky, D. V.; Bushinsky, M. V.; Sikolenko, V.; Efimov, V.; Cervellino, A. The low temperature macroscopic phase separation in $La_{0.5}Ba_{0.5}CoO_{3-\delta}$ cobaltite. *JETP Lett.* **2011**, *93*, 139−143.

https://dx.doi.org/10.1021/acs.jpclett.0c01919
J. Phys. Chem. Lett. 2020, 11, 6785−6790